Biosynthesis and Properties of Poly(3-hydroxybutyrate-*co*-3-hydroxyhexanoate) Polymers

Jawed Asrar,*,† Henry E. Valentin,† Pierre A. Berger,‡ Minhtien Tran,‡ Stephen R. Padgette,‡ and Joel R. Garbow†,§

Monsanto Company, 800 North Lindbergh Boulevard, St. Louis, Missouri 63167, and Monsanto Company, 700 Chesterfield Parkway North, St. Louis, Missouri 63198

Received March 27, 2002; Revised Manuscript Received June 17, 2002

In support of programs to identify polyhydroxyalkanoates with improved materials properties, we report on our efforts to characterize the mechanical and thermal properties of copolyesters of 3-hydroxybutyrate (3HB) and 3-hydroxyhexanoate (3HHx). The copolyesters, having molar fraction of 3HHx ranging from 2.5 to 35 mol % and average molecular weights ranging from 1.15×10^5 to 6.65×10^5, were produced by fermentation using *Aeromonas hydrophila* and a recombinant strain of *Pseudomonas putida* GPp104. The polymers were chloroform extracted and characterized by solution-state and solid-state nuclear magnetic resonance (NMR) spectroscopy and a variety of mechanical and thermal tests. Solution-state ^{1}H NMR data were used to determine polymer composition-of-matter, while solution-state ^{13}C NMR data provided polymer-sequence information. Solvent fractionation and NMR spectroscopic characterization of these polymers showed that polymers containing up to 9.5 mol % 3HHx had a Bernoullian compositional distribution. By contrast, polymers containing more than 9.5 mol % 3HHx had a bimodal polymer composition. Solvent fractionation of these 3HHx-rich polyesters produced two polymer fractions, each of which was again consistent with Bernoullian polymerization statistics. Solid-state NMR relaxation experiments provided insight into aging in poly(3HB-*co*-3HHx) copolymers, demonstrating increased polymer-chain motion with increasing 3HHx content. The elongation-to-break ratio in the polyesters increased with increasing molar fraction of 3HHx monomers. Aging properties of the poly(3HB-*co*-3HHx) copolymers were very similar to copolymers of 3HB and 3-hydroxyvalerate (3HV). However, poly(3HB-*co*-3HHx) exhibited increased activation energy to thermal degradation with increasing 3HHx content.

Introduction

Polyhydroxyalkanoates (PHAs) represent a diverse group of bacterial storage compounds commonly accumulated when carbon and energy sources are available in excess, but growth is limited by the lack of an essential nutrient.[1,2] These biological storage polyesters have many useful thermoplastic properties. Because they are produced from renewable resources and biodegrade to carbon dioxide and water,[3] PHAs are often described as environmentally friendly plastics. However, material characteristics, including low thermal stability,[4,5] which can affect polymer processing, and a slow and prolonged crystallization, leading to the formation of large spherulites,[6,7] limit the application of PHAs. Low temperature and solvent-based processes are therefore very desirable for this class of polymer. PHAs with lower melting point, lower crystallinity, and improved solubility have been the focus of research in different groups.[8−12] Copolymerization of 3-hydroxybutyrate (3HB) and 3-hydroxyvalerate (3HV) addresses some of these issues. Poly(3HB-*co*-3HV), however, is a relatively unusual copolymer because the 3HB and the 3HV units are isodimorphous, i.e., the similarity in the shape and size of these two monomers allows their incorporation into the same crystalline lattice without distortion of the lattice parameters.[13,14] Due to isodimorphism, many of the usual benefits of copolymerization are not realized. To produce PHAs with improved solubility and improved ductility, copolymerization of 3HB with longer chain hydroxyalkanoic acids, which cannot fit into each other's crystalline lattice and which therefore avoid isodimorphism, has been investigated.[9,12,15−17] This paper describes the microbial synthesis, characterization, and materials properties of copolymers of 3HB and 3-hydroxyhexanoate (3HHx), whose structural formula is shown in Chart 1, produced using *Aeromonas hydrophila* ATCC 14715 and recombinant *Pseudomonas putida* GPp104.

* To whom correspondence may be addressed. Phone: +1 (314) 694 1291. Fax: +1 (314) 694 3688. E-mail: jawed.asrar@monsanto.com.

† Monsanto Company, 800 N. Lindbergh Blvd.

‡ Monsanto Company, 700 Chesterfield Parkway North.

§ Current address: Department of Chemistry and Biomedical MR Laboratory, Washington University, Campus Box 8227, 4525 Scott Ave, St. Louis, MO 63110.

Experimental Section

(1) Polymer Synthesis. Bacterial Strains and Growth Conditions. *A. hydrophila* ATCC 14715 and *P. putida* strain GPp104 harboring plasmid pMON25806[18] were grown at 30 °C in nutrient broth or mineral salts medium[19] supplemented with an appropriate carbon source. Hoagland's trace element solution, used in the original mineral salts medium described by Schlegel et al.,[19] was replaced by trace element

10.1021/bm025543a CCC: $22.00 © 2002 American Chemical Society
Published on Web 08/21/2002

Chart 1

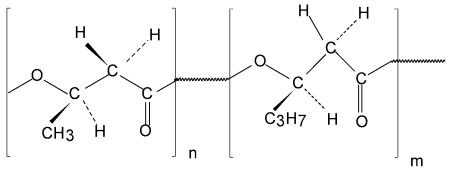

solution SL6.[20] As necessary, kanamycin was supplied at 100 mg/L for plasmid stabilization. For small-scale fermentations, cells were grown in a Braun Biostat B, 2 L, or a 10 L fermentor, containing 4 g of NH_4SO_4, 2.2 g of $MgSO_4 \cdot 7H_2O$, 1.7 g of citric acid, and 10 mL of trace-element solution (containing 10 g of $FeSO_4 \cdot 7H_2O$, 2.25 g of $ZnSO_4 \cdot 7H_2O$, 0.5 g of $CuSO_4 \cdot 5H_2O$, 2 g of $CaCl_2 \cdot 2H_2O$, 0.1 g of H_3BO_3, 0.1 g of $(NH_4)_6Mo_4O_{24}$, and 10 mL of HCl in 1 L) per liter. After autoclaving, this medium was supplemented with 3.5 g of KH_2PO_4/L and an appropriate carbon source. During fermentation, the pH was maintained at pH 6.8 using ammonia and 20% sulfuric acid. For aeration, 4 L of air was passed through the fermentor per minute, at an agitation rate of 730−1200 rpm (max dissolved oxygen = 20%). Fermentations were performed at 30 °C using 1% volume of an overnight preculture as inoculum.

(2) Polymer Characterization. (a) Solution-State Nuclear Magnetic Resonance (NMR) Spectroscopy. Solution state ^1H and ^{13}C NMR spectra were acquired using Varian spectrometers (Varian NMR Instruments, Palo Alto, CA) operating at 300, 400, and 500 MHz ^1H frequency. The 400 and 500 MHz instruments were equipped with 5-mm, indirect-detection probes, and the 300 MHz instrument was equipped with a four-nucleus probe. In addition, the 400 MHz spectrometer was equipped with a 10 mm direct-detection probe for ^{13}C observation. Peak areas were determined by direct integration (^1H spectra) or with the help of a peak deconvolution program for overlapping dyad and triad components (^{13}C spectra). Other computations were performed with Excel version 4.0 spreadsheets.

(b) Solid-State NMR Spectroscopy. Cross-polarization magic-angle spinning (CP-MAS) ^{13}C NMR spectra were collected on a Monsanto-built spectrometer operating at a proton resonance frequency of 127.0 MHz. Samples were spun at the magic angle with respect to the magnetic field in a double-bearing rotor system at a rate of 3 kHz. CP-MAS ^{13}C NMR spectra were obtained at 31.9 MHz following 2-ms matched, 50 kHz $^1H-^{13}C$ cross-polarization contacts. High-power proton dipolar decoupling ($H_1(H) = 65$ kHz) was used during data acquisition. Under these conditions, the relative intensities of the peaks observed in each of the spectra reflect accurately the relative amounts of each carbon type present in the samples.

(c) Molecular-Weight Determination. Molecular weights were determined by gel permeation chromatography (GPC) using a Waters 515 HPLC pump, connected to 10^3, 10^4, 10^5, and 10^6 Å Waters Ultrastyragel columns (7.8 × 300 mm) placed in series. The detection system consisted of a Waters 410 differential refractometer and a Viscotek T50 dual capillary viscometer connected in parallel. Chloroform was the eluent, at a flow rate of 1.0 mL/min. Typical sample volumes were 100 μL at a polymer concentration of 2 mg/mL. Samples were prepared using a stock solution of chloroform containing 1,2,4-trichlorobenzene (350 μL in 430 mL of chloroform) as a flow-rate marker. Narrow polydispersity polystyrene standards (Toyo Soda, Japan) were used to generate a universal calibration curve, from which the molecular weights were determined, after correcting for flow-rate variations based on the elution volume of the flow-rate marker.

(d) Measurement of Thermal Properties. Glass-transition temperatures, heats of fusion, and melting temperatures were measured on a Perkin-Elmer DSC-7. Approximately 10 mg samples, annealed at 75 °C for 30 min, were encapsulated in standard aluminum differential scanning calorimetry (DSC) pans and heated from −50 to 180 °C. Heating and cooling rates were 20 °C/min. The midpoint of the total change in heat capacity was designated as the glass-transition temperature and the peak temperature as the melting point. All calculations were performed on the first heating cycle. A pure indium metal was used to determine the temperature correction factor.

(e) Isothermal Thermogravimetric Analysis (TGA). Samples, in powder form, were tested by simultaneous differential thermal analysis thermogravimetric analysis (DTA-TGA) using an Omnitherm STA 1500 thermogravimetric analyzer and analyzed using the accompanying software package. The instrument weight axis was calibrated according to the instrument standard operating procedure. The TGA module measures weight loss as a function of temperature through the use of a null seeking balance. The furnace was calibrated using a number of temperature stability readings at 2 °C intervals. The procedure followed in the analysis involved heating a series of four, 5 ± 1 mg samples isothermally at 200 °C. The samples were heated from 25 °C and maintained at 200 °C for 120 min, and the weight lost over time was recorded.

(f) Determination of the Activation Energy of Thermal Degradation by TGA. Samples, in powder form, were tested by simultaneous DTA-TGA as described above. The procedure followed in the analysis was based on ASTM Standard E 1641-94 (Standard Test Method for Decomposition Kinetics by Thermogravimetry) and involved heating a series of four samples (5 ± 1 mg) at heating rates of 1, 2, 5, and 10 K/min. Samples were heated from 25 °C through decomposition (from 230 to 310 °C). The temperature at which the sample lost 10% of its weight was recorded for each of the four rates. The slope of the Arrhenius plot, log(heating rate (K/min)) vs 1/temperature (K), was determined by least-squares fit and used to calculate the activation energy.

Results and Discussion

Biosynthesis and Microstructure of Poly(3-hydroxybutyrate-*co*-3-hydroxyhexanoate) Polymers. Table 1 summarizes materials properties for poly(3-hydroxybutyrate-*co*-3-hydroxyhexanoate) [poly(3HB-*co*-3HHx)] copolymers with 3HHx molar fractions ranging from 2.5 to 35 mol %. Polymers with molar fractions of 3HHx ranging from 2.5 to 9.5 mol % were obtained using *Aeromonas hydrophila* for

Table 1.

bacterial strain for production	harboring plasmid	carbon source	3HHx content (mol %)	M_w	M_w/M_n	crystal growth rate (G, μm/s)	$t_{1/2}$ (min)	ΔH (J/g)	tensile properties: elongation to break (%)	tensile properties: strength (Map)	tensile properties: modulus (GPa)
A. hydrophila 7966		wheatgerm oil	2.5	231 000	2.50	1.571	0.97	66.7	6.7	25.7	631.3
A. hydrophila 14715		soybean oil/3HB	4.0	170 000	2.20						
A. hydrophila 14715		soybean oil/3HB	4.6	115 000	2.10	1.272	0.36	66.9	6.5	22.9	599.9
A. hydrophila 14715		soybean oil	5.4	401 000	2.30	0.525	1.77	54.7	17.6	23.9	493.7
A. hydrophila 14715		soybean oil/3HB	5.9	665 000	2.90	0.297	1.09	54.0	163.0	17.7	412.3
A. hydrophila 14715		soybean oil	6.3	375 000	2.50	0.335	1.82	54.4	24.0	17.9	342.6
A. hydrophila 14715		soybean oil	7.0	548 000	2.60	0.259	4.84	49.9	23.6	17.3	288.9
A. hydrophila 14715		soybean oil/3HB	8.4	427 000	2.33	0.082	2.60	42.3	11.9	14.5	898.0
A. hydrophila 14715		soybean oil/capronate	8.5	246 000	2.30	0.096	4.15	38.1	25.1	17.8	249.6
A. hydrophila 14715		soybean oil/capronate	8.5	366 000	3.20	0.072	5.66	35.6	34.3	15.6	232.3
A. hydrophila 14715		rape seed oil	9.5	543 000	3.50	0.054	3.33	37.8	43.0	8.8	155.3
P. *putida* GPp104	pMON25806	butyrate/capronate	19.0	588 000	1.84		4.33	19.9			
P. *putida* GPp104	pMON25806	capronate	26.0	259 000	2.26		2.43	2.6			
P. putida GPp104	pMON25806	butyrate/capronate	32.0	437 000	1.78		6.85				
P. *putida* GPp104	pMON25806	oleate/capronate	35.0	376 000	1.64		1.89				

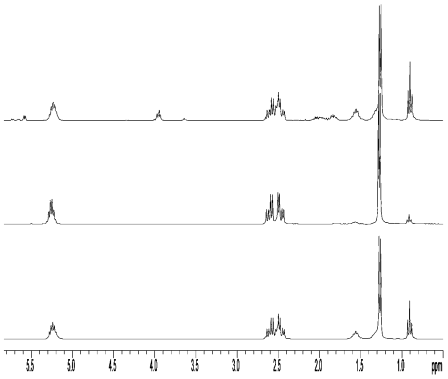

Figure 1. Solution-state ^{1}H NMR spectra of poly(3HB-*co*-3HHx) with 25.7 mol % 3HHx: (bottom) polymer before fractionation; (middle) hexane-insoluble fraction containing 6.9 mol % HHx; and (top) hexane-soluble fraction containing 33.6 mol % HHx.

fermentations. Polymers containing more than 9.5 mol % 3HHx were obtained using *Pseudomonas putida* GPp104 (pMON25806). Fermentation experiments were performed in a Braun Biostat B, 2 L, or a 10 L fermentor. Application of wheatgerm oil, soybean oil, rapeseed oil, hexanoate and 3HB as carbon sources in various combinations did not significantly affect the polymer composition. The polymers were purified by chloroform extraction and ethanol precipitation prior to further characterization. The compositions of the samples (i.e., molar fractions 3HHx and 3HB) were calculated from ^{1}H peak integrals.

Figure 1 shows ^{1}H NMR spectra of poly(3HB-*co*-3HHx) samples. In these ^{1}H spectra, the H_4 and H_6 peaks of 3HHx (chemical shifts 1.55 and 0.90 ppm, respectively) were individually resolved; all other partial integrals were sums of 3HB and 3HHx intensities.

In contrast to the ^{1}H NMR spectrum, the ^{13}C NMR spectrum contains compositional sequence information in the form of resolved dyads and triads.[21−23] Figure 2, the ^{13}C spectra of the carboxyl (C_1) resonance of poly(3HB-*co*-3HHx), is separated into three dyad components, from low to high field, c*c, [c*b, b*c], b*b, where c refers to 3HHx units and b to 3HB units. Some less clearly resolved tetrad splitting is also apparent in these spectra. The 3HHx C2 and C4 peaks were split into triads, from low to high field, bc*b, [cc*b, bc*b], cc*c. The other ^{13}C peaks did not display sufficiently well resolved fine structure to provide compositional sequence information. By comparing calculated peak intensities with the experimental peak intensities of assigned compositional dyads and triads for C1, C2, and C4, we were able to verify a given type of polymerization statistics. Polymers from the *A. hydrophila* production system, which contained up to 9.5 mol % 3HHx, had Bernoullian compositional distributions. Polymers from the *A. putida* production system, which contained more than 9.5 mol % 3HHx, were bimodal. This was surprising in view of the narrow molecular-weight distribution. Bimodal character was initially deduced from the observation that the deconvoluted peak intensities of the assigned dyads and triads could not be fitted to Bernoullian or first-order Markovian distributions but were reasonably well modeled as the sum of two Bernoullian distributions. To better characterize the bimodal nature of these samples, we physically separated the polymers by taking advantage of the different solution properties of 3HB and 3HHx (see Polymer Characterization). The polymer containing 25.7 mol % 3HHx was fractionated. The hexane-soluble copolymer fraction was enriched in 3HHx, 33.6 mol %, while the hexane-insoluble copolymer fraction was depleted in 3HHx, 6.9 mol %. This calculated to 70% hexane soluble polymer, in close agreement with the material balance, 75%. Both fractions obeyed Bernoullian statistics with less than 1% deviation. Whether bimodality is a result of the polymer composition or is a characteristic of the *P. putida* PHA production system remains unclear at this time.

Properties of Poly(3-hydroxybutyrate-*co*-3-hydroxyhexanote). Incorporation of 2.5 to 9.5 mol % 3HHx into poly(3HB-*co*-3HHx) caused considerable changes in bulk and solution properties. In contrast to poly(3HB) or poly(3HB-*co*-3HV), copolymers containing as low as 2.5 mol % 3HHx were soluble in amide solvents such as dimethyl acetamide (DMAC) and *N*-methyl pyrrolidinone (NMP). Thermal properties were similarly affected by the incorpora-

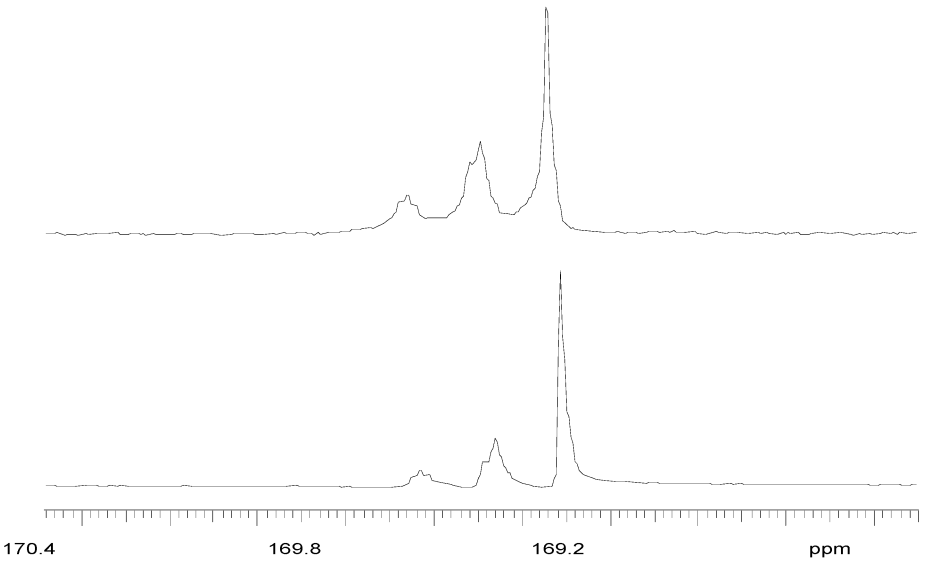

Figure 2. Carbonyl (C_1) region of solution-state ^{13}C NMR spectra of poly(3HB-*co*-3HHx): (bottom) polymer before fractionation containing 27.7 mol % 3HHx; (top) hexane-soluble fraction containing 33.6 mol % 3HHx.

tion of 3HHx in the polymer. DSC thermograms of all the copolymers studied showed the presence of two distinct endotherms, attributed to polymorphism, as has been observed in other aliphatic polyesters. Presence of multiple endotherms could arise either due to compositional heterogeneity, multiple crystalline forms, or simply due to recrystallization during the heating runs in the DSC. Thermal properties of well-fractionated poly(3HB-*co*-3HHx) were published recently, and it was clearly demonstrated that in poly(3HB-*co*-3HHx), with 3HHx content of less than 20 mol %, the high-temperature peak in DSC is due to the recrystallization during heating where the copolymer chains have enough time to rearrange to better crystal packing.[15] Thermal history of the material is known to effect the melting behavior of several semicrystalline polymers.[15,17,24,25] To avoid the effects arising due to differences in the thermal history of each polymer sample, it was decided to anneal the polymers at 75 °C before analyzing for the thermal behavior using DSC. Both melting point peaks were present in all poly(3HB-*co*-3HHx) copolymers tested (Figure 3, bottom). Incorporation of 3HHx into the polymer had an impact on both endotherms, and both moved to lower temperatures as the molar fraction of 3HHx monomer in poly(3HB-*co*-3HHx) increased. The crystallinity, as measured by the enthalpy of fusion, ΔH, of the two melting peaks decreased with increasing amounts of 3HHx in the copolymer. (Table 1/Figure 3, middle). Consistent with the effects of 3HHx on the fusion enthalpy, the crystallization 1/2 time ($t_{1/2}$) increased with increasing levels of 3HHx in the polymer (Table 1/Figure 3, top). The data are more scattered for copolymers with higher levels of 3HHX probably because the presence of minute amounts of impurities acting as nucleating agents will have more impact on copolymers, which are slow to crystallize. A trend toward higher $t_{1/2}$ values with increasing molar fractions of 3HHx, however, is clearly observed.

The effect of 3HHx on spherulite morphology was studied with a polarized optical microscope. Polymer samples were crystallized isothermally at 75 °C without addition of nucleating agents, and optical micrographs of poly(3HB-*co*-3HHx) samples were collected. Figure 4 shows typical spherulite structures of poly(3HB-*co*-3HHx) samples containing 2.5, 4.6, and 9.5 mol % 3HHx. The micrographs show a reduction in the spherulite size and an increase in the regular banding pattern with increasing molar fractions of 3HHx.

The effect of 3HHx on the mechanical properties of the copolymers was studied on micrometer-thick films produced by melt casting. In agreement with results reported by Doi et al.,[12] the incorporation of 3HHx units into poly(3HB) improved elongation-to-break ratio (Figure 5); error bars are much longer for copolymer with higher concentrations of 3HHX because the presence of defects and impurities in a ductile material leads to large differences between samples. As reported in Table 1, these improvements were accompanied by a decrease in modulus. In contrast to data reported by Doi et al., who found elongation-to-break ratios of several hundred percent for comparable polymers,[12] maximum elongation-to-break levels for poly(3HB-*co*-3HHx) copolymers were only 40% (copolymer containing 9.5 mol % 3HHx). The reason for differences in these data is not known but may be a manifestation of variations in crystal morphology. Such variations are not surprising, since Doi analyzed solvent-cast films while we studied thermally processed films in this work.

In an effort to gain further insight into the effect of 3HHx units on the structure and bulk properties, copolymers containing 5.2, 5.8, 7.4, and 9.3 mol % 3HHx were investigated by CP-MAS ^{13}C NMR. Polymers in the solid state are undergoing motions, over a wide range of frequencies. Different frequency regimes can be investigated with different solid-state NMR relaxation experiments. Proton and carbon rotating-frame relaxation, $T_{1\rho}(H)$ and $T_{1\rho}(C)$, help to probe low-frequency (kHz regime), cooperative polymer-chain motions. The effects of 3HHx units and the aging of the copolymer can therefore be studied.

The CP-MAS ^{13}C NMR spectrum of poly(3HB-*co*-3HHx) gave four sharp lines at chemical shifts of 21, 43, 68, and 170 ppm due to the carbons in poly(3-hydroxybutyrate).

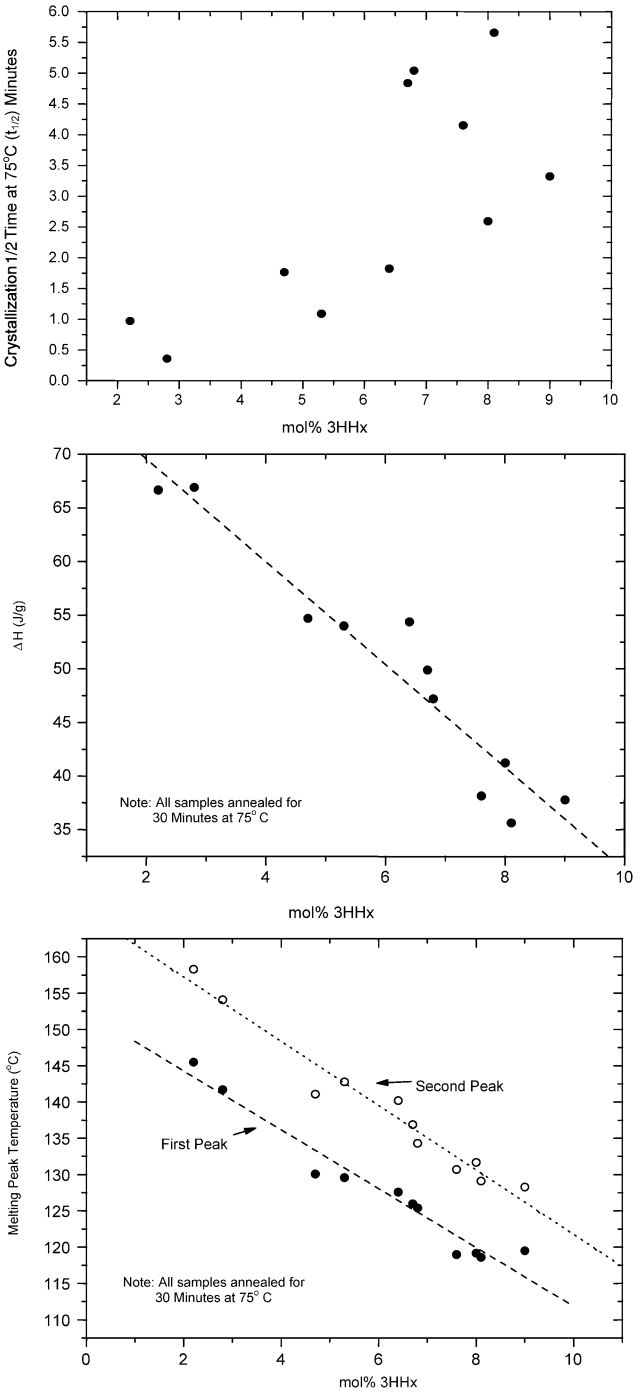

Figure 3. Melting temperature (bottom), fusion enthalpy, ΔH (middle), and crystallization 1/2 time ($t_{1/2}$) as a function of 3HHx content, in a series of poly(3HB-*co*-3HHx) samples. All samples were annealed for 30 min at 75 °C.

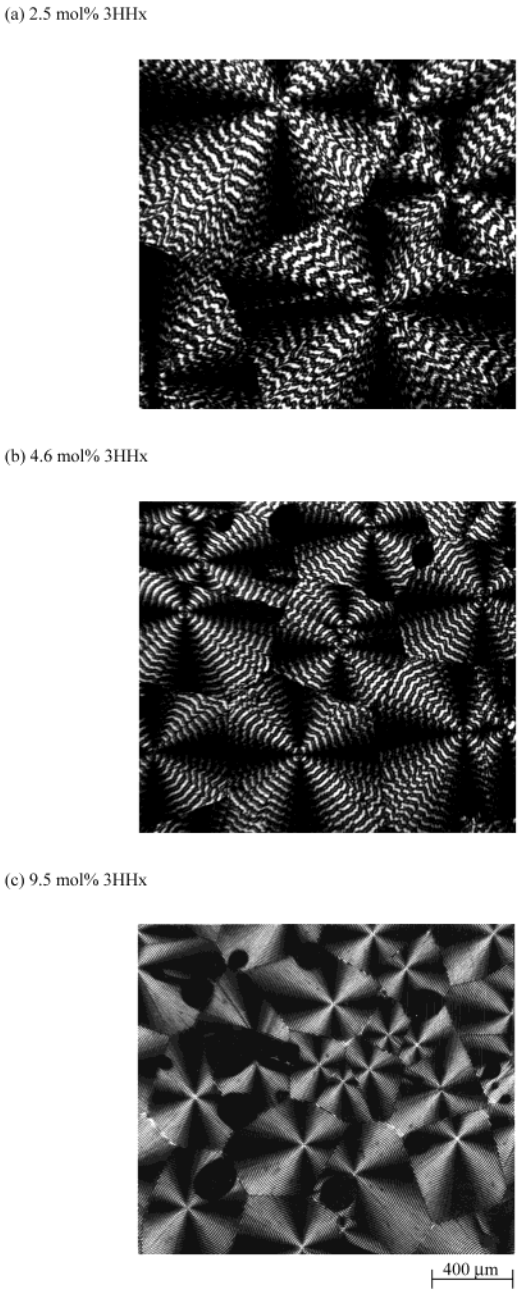

Figure 4. Polarized optical micrographs of poly(3HB-*co*-3HHx), showing crystal structure and spherulite size, for polymers containing (a) 2.5, (b) 4.6, and (c) 9.5 mol % 3HHx, respectively.

Figure 6 shows the CP-MAS ^{13}C NMR spectrum of poly(3HB-*co*-3HHx) containing 5.4 mol % 3HHx, which is typical of all the (3HB-*co*-3HHx) investigated in this paper. The resonance at 14 ppm due to the methyl group of the 3HHx unit was the only resolved signal from this moiety. A series of relaxation experiments to measure proton rotating-frame relaxation, $T_{1\rho}(H)$ were performed. Proton rotating-frame relaxation times were determined from the decay of carbon signal as a function of $^1H-^{13}C$ contact time, τ, in a CP-MAS experiment. The value $T_{1\rho}(H)$ is calculated from a straight-line fit of log(carbon signal intensity) vs τ, where τ varies from 2 to 12 ms. The decay curves of ^{13}C signal vs contact time (raw data not shown) were well fit as single exponentials and showed no evidence of two-component (biexponential) behavior. Table 2 summarizes the results of these $T_{1\rho}(H)$ experiments.

Table 2. Proton Rotating-Frame Relaxation and Activation Energy for Thermal Degradation as a Function of 3HHx Content in Poly(3HB-co-3HHx)

% HHx	$\langle T_{1\rho}(H)\rangle$ (ms)	activation energy (kJ/mol)
5.2	21	100
5.8	20	110
7.2	16	118
9.0	15	120

The rotating-frame relaxation data in Table 2 show a clear trend toward shorter $T_{1\rho}(H)$ values with increasing % 3HHx, indicating increased kilohertz-regime motions of the polymer

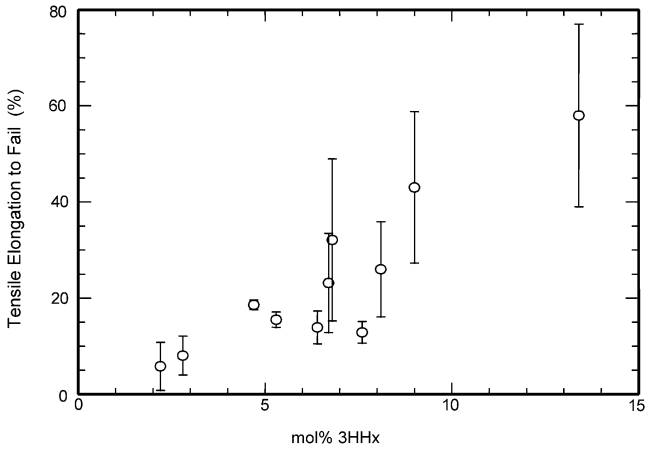

Figure 5. Percent tensile elongation to break, as a function of 3HHx level, in a series of poly(3HB-*co*-3HHx) samples.

chains in copolymers having higher 3HHx content. The observed trend in $T_{1\rho}$(H) is indicative of disruption in crystallinity caused by 3HHx units, leading to higher amorphous content in the polymer. Exclusion of 3HHx units from the crystalline lattice of P(3HB), resulting in decreased crystallinity and reduced rate of crystallization, in P(3HB-*co*-3HHx) copolymers, was also demonstratedusing 2D Fourier transform infrared correlation spectroscopy.[17]

Thermal stability of PHAs is of particular importance. PHAs with low melting temperatures and/or increased thermal stability are desirable. The thermal stability of P(3HB), and copolymers P(3HB-*co*-3HV) and P(3HB-*co*-3HHx), containing 30 mol % 3HV and 15 mol % 3HHx was recently investigated using dynamic TGA, and it was found that copolymers degraded slower than the homopolymer.[16] The thermal stability of poly(3HB-*co*-3HHx) poly-

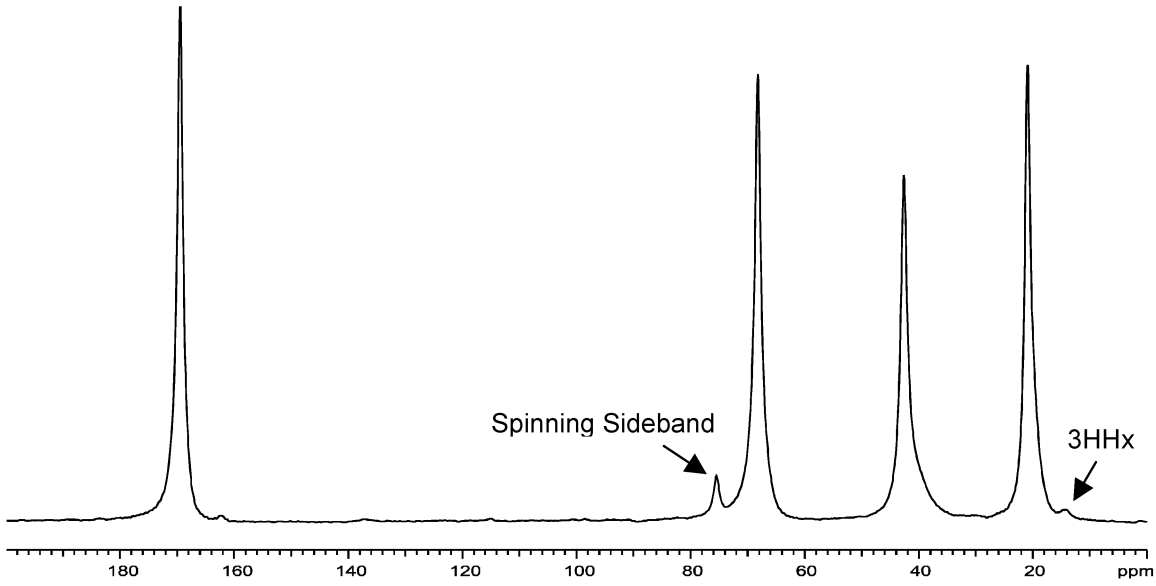

Figure 6. Cross-polarization magic-angle spinning ^{13}C NMR spectrum of poly(3HB-*co*-3HHx) containing 5.4 mol % 3HHx.

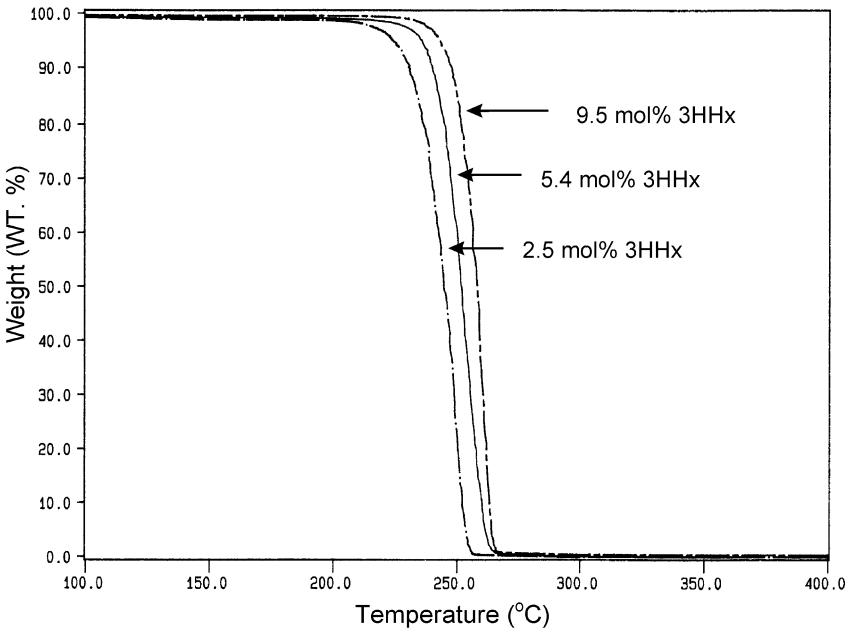

Figure 7. Weight loss vs temperature for a series of thermally cast films of poly(3HB-*co*-3HHx) containing 2.5, 5.4, and 9.5 mol % 3HHx units.

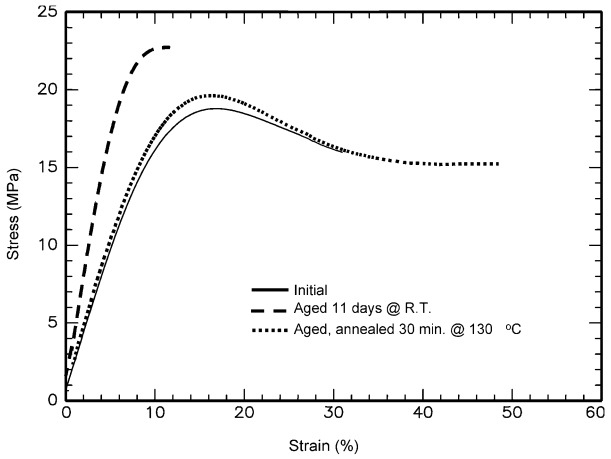

Figure 8. Stress vs strain curves for poly(3HB-*co*-3HHx) copolymer containing 8.1 mol % 3HHx units.

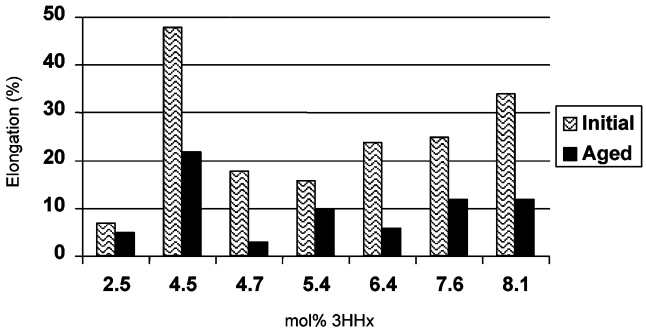

Figure 9. Effect of aging on percent elongation of thermally cast films of poly(3HB-*co*-3HHx) containing different levels of 3HHx.

esters reported here was measured by TGA. Figure 7 shows TGA thermograms of several copolymers, containing different levels of 3HHx units, determined at 20 °C/min in nitrogen atmosphere. The temperature at which weight loss starts increases with increasing amount of 3HHX in the copolymer. Activation energy for thermal degradation, as measured by isothermal TGA, is also found to increase with increasing levels of 3HHx (Table 2, column 3).

Thermal degradation in poly(3HB) is known to take place by random chain scission, in which the degradation starts with the formation of a six-membered ring and C−C bond breakage of the polymer main chain is accompanied by the elimination of β-hydrogen.[4,5] Increases in thermal stability of poly(3HB-*co*-3HHx) polyesters may be a result of *steric* hindrance to the formation of six-membered rings created by the propyl side chain of 3HHx. It is interesting to note that like thermal degradation, resistance to enzymatic degradation also increases with the incorporation of 3HHx units in the polymer.[12]

Poly(3HB) and poly(3HB-*co*-3HV) are known to undergo secondary crystallization, which reduces the number of polymer chains in the amorphous phase, resulting in a detrimental embrittlement of the material.[6,7] It was believed that poly(3HB-*co*-3-hydroxyalkanoate) copolymers containing longer chain 3-hydroxyalkanoate comonomers that do not cocrystallize would exhibit minimal secondary crystallization and, hence, no significant aging. However, in our hands poly(3HB-*co*-3HHx) of all tested compositions exhibited the typical signs of polymer aging. Figure 8 presents the stress-versus-strain curve for a poly(3HB-*co*-3HHx) sample containing 8.1 mol % 3HHx. While the initial sample exhibited elongation of 31.6% and strength of 18.8 MPa, the elongation was reduced to 12% and the strength increased to 22.8 MPa after 11 days of room-temperature aging. As shown in Figure 9, all poly(3HB-*co*-3HHx) copolymers exhibited a reduction in elongation-to-break and an increase in modulus over time, similar to poly(3HB) homopolymers.[6] Freshly prepared and 3-months-aged films of poly(3HB-*co*-3HHx) containing 9 mol % 3HHx were investigated by CP-MAS ^{13}C NMR. $T_{1\rho}$(H) decreased from 15 to 13 ms, indicating reduced molecular motion in the aged samples. Annealing reduced the aging process. An 11-day-aged film of poly(3HB-*co*-3HHx) with 12% elongation and 22.8 M Pa strength exhibited an elongation of 50% and strength of 19.6 M Pa following annealing at 130 °C for 30 min. Reaging of the annealed polymer again occurs, however.

Acknowledgment. We thank Gerald Hook, Devang Shah, Deborah Johnson, and Vladimir Bekker for polymer separation, GPC, and thermal analysis, Paul Garrett and Jeff Hurlbut for evaluation of mechanical properties, David Snyderman for CP-MAS ^{13}C NMR spectroscopy, and Ken Gruys for useful discussions.

References and Notes

(1) Anderson, A. J.; Dawes, E. A. *Microbiol. Rev.* **1990**, *54*, 450.
(2) Steinbüchel, A.; Valentin, H. E. *FEMS Microbiol. Lett.* **1995**, *128*, 219.
(3) Müller, H. M.; Seebach, D. *Angew. Chem.* **1993**, *105*, 483.
(4) Grassie, N.; Murray, E. J.; Holmes, P. A. *Polym. Degrad. Stab.* **1984**, *6*, 95.
(5) Spyros, A.; Argyropoulos, D. S.; Marchessault, R. H. *Macromolecules* **1997**, *30*, 327.
(6) de Koning, G. J. M.; Scheeren, A. M. C.; Lemstra, P. J.; Preeters, M.; Reynears, H. *Polymers* **1994**, *35*, 4598−4605.
(7) de Koning, G. J. M.; Lemstra, P. J.; Hill, D. J. T.; Carswell, T. G.; O'Donnell, J. H. *Polymers* **1992**, *33*, 3295−97.
(8) Foster, L. J. R.; Zervas, S. J.; Lenz, R. W.; Fuller, R. C. *Biodegredation* **1995**, *6* (1), 67−73.
(9) Carmen, S.; Wolk, S.; Lenz, R. W.; Fuller, R. C. *Macromolecules* **1994**, *27* (22), 6358−62.
(10) Valentin, H. E.; Berger, P. A.; Gruys, K. J.; de Andrade Rodrigues, M. F.; Steinbüchel, A.; Tran, M.; Asrar, J. *Macromolecules* **1999** *32* (22), 7389−7395.
(11) Saito, Y.; Doi, Y. *Int. J. Biol. Macromol.* **1994**, *16*, 99.
(12) Doi, Y.; Kitamura, S.; Abe, H. *Macromolecules* **1995**, *28*, 4822.
(13) Scandola, M.; Eccorulli, G.; Pizzoli, M.; Gazzano, M. *Macromolecules* **1992**, *25*, 1405.
(14) Bluhm, T. L.; Hamer, G. K.; Marchessault, R. H.; Fyfe, C. A.; Veregin, R. P. *Macromolecules* **1986**, *19*, 2871.
(15) Wantanabe, T.; He, Y.; Fukuchi, T.; Inoue, Y. *Macromol. Biosci.* **2001**, *1*, 75.
(16) He, J.-D.; Chenng, M. K.; Yu, P. H.; Chen, G. *J. Appl. Polym. Sci.* **2001**, *82*, 90.
(17) Tian, G.; Wu, Q.; Sun, S.; Noda, I.; Chen, G.-Q. *J. Polym. Sci., Polym. Phys.* **2002**, *40*, 649.
(18) Clemente, T.; Shah, D.; Tran, M.; Stark, D.; Padgette, S.; Dennis, D.; Brückner, K.; Steinbüchel, A.; Mitsky, T. *Appl. Mircobiol. Biotechnol.* **2000**, *53*, 420.
(19) Schlegel, H. G.; Lafferty, R.; Krauss, I. *Arch. Mikrobiol.* **1970**, *71*, 283.
(20) Pfennig, N. *Arch. Microbiol.* **1974**, *100*, 197.
(21) Shimamura, E.; Kasuya, K.; Kobayashi, G.; Shiotani, T.; Shima, Y.; Doi, Y. *Macromolecules* **1994**, *27*, 878.
(22) Doi, Y.; Kunioka, M.; Nakamura, Y.; Soga, K. *Macromolecules* **1986**, *19*, 2860.
(23) Bloembergen, S.; Holden, D.; Bluhm, T. L.; Hamer, G. K.; Marchessault, R. H. *Macromolecules* **1987**, *20*, 3086.
(24) Marco, C.; Lazeano, S.; Faton, J. G. *Makromol. Chem.* **1990**, *191*, 1151.
(25) Pearce, R.; Marchessault, R. H. *Polymer* **1994**, *35*, 3990.

BM025543A